Numerical study on pressure fluctuation of a multistage centrifugal pump based on whole flow field

Cite as: AIP Advances **9**, 035118 (2019); https://doi.org/10.1063/1.5049196
Submitted: 20 July 2018 • Accepted: 28 February 2019 • Published Online: 13 March 2019

Chuan Wang, Xiaoke He, Weidong Shi, et al.

Numerical study on pressure fluctuation of a multistage centrifugal pump based on whole flow field

Cite as: AIP Advances 9, 035118 (2019); doi: 10.1063/1.5049196
Submitted: 20 July 2018 • Accepted: 28 February 2019 •
Published Online: 13 March 2019

Chuan Wang,[1] Xiaoke He,[2] Weidong Shi,[3] Xikun Wang,[1,4,a)] Xiuli Wang,[4] and Ning Qiu[1,4,a)]

AFFILIATIONS

[1]School of Hydraulic, Energy and Power Engineering, Yangzhou University, Yangzhou, Jiangsu Province 225002, China
[2]School of Electric Power, North China University of Water Resources and Electric Power, Zhengzhou, Henan Province 450045, China
[3]School of Mechanical Engineering, Nantong University, Nantong, Jiangsu Province 226019, China
[4]Research Center of Fluid Machinery Engineering and Technology, Jiangsu University, Zhenjiang, Jiangsu Province 212013, China

[a)]**Corresponding author. E-mail address:** qiuning@ujs.edu.cn (N. Qiu), wangxk@ujs.edu.cn (X. Wang)

ABSTRACT

Multistage centrifugal pumps can provide high-pressure fluid flow, and is widely used in various engineering applications. However, the pressure fluctuation in the pumps strongly affects the flow and pressure stability. To gain further insight into the pressure fluctuation of multistage centrifugal pumps, a numerical model of a typical multistage centrifugal pump model was constructed and the flow investigated systematically under different operating conditions. Changes in amplitude, frequency, and phase of pressure fluctuation in the impellers, diffusers, and pump cavities were observed and analyzed in both time-domain and frequency-domain. The pressure fluctuations of the fluid in the impeller were found to originate from the inlet side of the outward diffuser, whereas that in the diffuser arose from the outlet side of the impeller blade. In contrast, the pressure fluctuations in the pump cavity were initiated from the outlet side of the impeller blade and the interstage leakage of fluid. This study also conclude that the pressure fluctuations are essentially a wave with identifiable amplitude, frequency, and phase.

I. INTRODUCTION

Multistage centrifugal pumps are widely used in various engineering sectors, such as oil, mining, power, and irrigation.[1–5] Any increase in the number of pump stages renders the instability of the multistage centrifugal pump system vital. However, the pressure fluctuation caused by the rotor-stator interaction (RSI) between the rotational impeller and the stationary diffuser may lead to strong vibration and noise in the multistage centrifugal pump during its operation. In extreme cases, a multistage centrifugal pump may be severely damaged and broken down. Therefore, an in-depth study of the pressure fluctuation is important for improving the stability of the pump. During the past two decades, it has become possible for one to investigate three-dimensional unsteady turbulent flow in pumps in greater details than before because of the advancement in computational fluid dynamics (CFD) and experimental techniques.[6–10]

Theoretically, RSI involves two kinds of flows phenomena, i.e., potential and wake flows.[11–13] Potential flow is associated with the inviscid flow due to the relative motion of the fluid between the rotating impeller and the stationary diffuser. By contrast, the wake flow arises from the flow separation from the impeller, thereby resulting in impact and convective flows. During the revolution of the impeller, RSI induces periodic flow and periodic pressure fluctuation. In view of the unsteady pressure fluctuation characteristics in pumps, several experiments have been conducted,[14–18] but the measured position was mainly limited near the inner wall surface of the pump. Hence, the measured results and the actual pressure

fluctuation characteristics noticeably differ. Moreover, the pressure fluctuation in the rotational impeller is difficult to measure, but it can be easily obtained through numerical simulation. Therefore, in comparison with test methods, the use of numerical calculation for obtaining the pressure fluctuation in pumps is more convenient and efficient.

With regard to the pressure fluctuation in the pump, most of the published numerical studies focus on the volute centrifugal pump,[19,20] axial-flow pump,[21,22] mixed-flow pump,[23,24] and turbine.[25,26] In comparison, little attention was paid to multistage centrifugal pump. Shi et al.[27] simulated the pressure fluctuation at the downstream of the impeller outlet in a diffuser pump using CFD; they found that RSI between the impeller and the diffuser is due to the impact of the wake flow on the diffuser. Liu et al.[28] studied the pressure fluctuation of radial diffusers in a multistage centrifugal pump, and showed that the impeller blade passing frequency has the strongest influence and the amplitude of pressure fluctuation is reduced gradually with an increase in the number of pump stages. Shi et al.[29] further investigated the transient operation characteristics of multistage submersible pumps, in which the pressure fluctuation at all the monitored points varied periodically. The pressure fluctuation's number of periods is strongly correlated with number of impeller blades but less affected by the number of diffuser blades. While most of the studies focused on the main flow parts of the pumps (such as the impellers, diffusers, and pump cavities), the volumetric leakage and interstage leakage have not been investigated. Moreover, the previous studies generally focused on the amplitude and frequency of the pressure fluctuation in the pump and paid insufficient attention to the internal influencing law between the amplitude, frequency, and phase of the pressure fluctuation wave. In this research, the phase of the pressure fluctuation wave in a multistage pump is to be investigated.

II. MODEL SETUP

A. Hydraulic design of the impeller and diffuser

In this study, a two-stage centrifugal pump was selected as the model. The core components of the pump include the impeller and diffuser, whose geometric parameters are calculated by using the velocity coefficient method, see Table I. The two-dimensional views of the impeller and diffuser are shown in Figures 1 and 2, respectively.

TABLE I. Basic geometric parameters of the pump.

Geometric parameter	Value
Inlet diameter of the impeller D_1 (mm)	20
Hub diameter of the impeller D_{hb} (mm)	33.5
Outlet diameter of the impeller D_2 (mm)	108
Inlet angle of the impeller blade β_1 (°)	40
Outlet angle of the impeller blade β_2 (°)	15
Wrap angle of the impeller blade θ_w (°)	150
Number of the impeller blades Z	8
Outlet width of the impeller blade b_2 (mm)	3
Number of the outlet diffuser blades Z_p	9
Number of the return diffuser blades Z_n	9
Inlet diameter of the outlet diffuser D_3 (mm)	109
Inlet angle of the outlet diffuser blade α_3 (°)	5
Outlet angle of the return diffuser blade α_6 (°)	50
Rated flow rate Q_r (m^3/h)	3.3

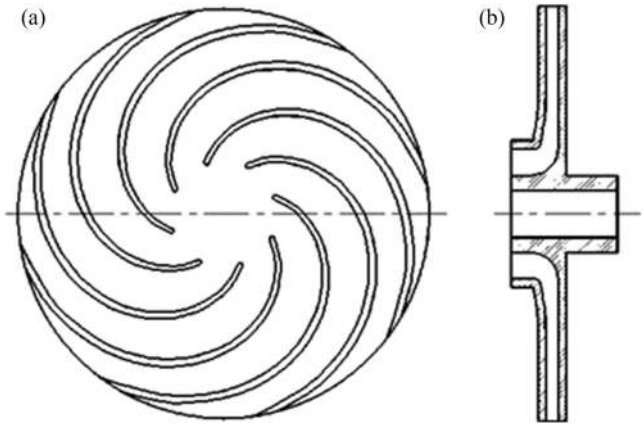

FIG. 1. Two-dimensional view of the impeller: (a) plane projection; (b) axial projection (8 blades).

B. Simulation domain

Figure 3 shows the simulation domain of the two-stage pump, which consists of the inlet section, two impellers, two pump cavities, two diffusers, two front rings, two rear rings, and the outlet section. Therefore, the energy losses in all components of the multistage pump have been considered.

C. Boundary conditions

The unsteady flow simulation was an extension of a steady state numerical simulation,[1] in which independence analysis of grid numbers, turbulence models, convergence precisions, and surface roughness had been carried out. The impeller and the shroud in the pump cavity were established based on the rotating reference frame, whereas the other subdomains were based on the stationary reference frame throughout the entire simulation domain. An open inlet and mass outflow were selected as the inlet and outlet boundaries,

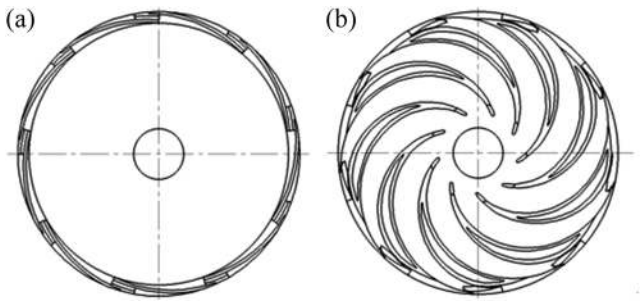

FIG. 2. Two-dimensional view of the diffuser: (a) outlet diffuser; (b) return diffuser (9 blades).

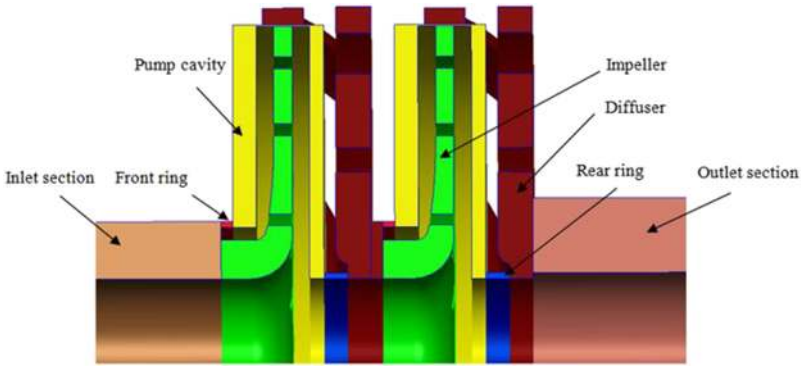

FIG. 3. Simulation domain of the two-stage pump.

respectively. Finally, the time step was chosen and set based on 1/360 of the period of the rotation of the impeller, the rotational speed of which was 2800 rpm.

D. Location of the monitoring points

Figure 4 (a) shows the eight monitoring points (I1 – I8) selected to retrieve the unsteady pressure and flow in the multistage pump. I1, I2, I3, and I4 were located along the middle streamline of an impeller flow channel and intersected with various radius R = 19.5, 31, 42.5, and 53.75 mm. I5, I6, I7, and I8 were the monitored points located close to the blade suction and pressure sides at the circles of radius R = 42.5 and 53.75 mm, respectively, in the same impeller flow channel. The monitoring points in the pump cavity (C1 – C15) are shown in Figure 4 (b). Points C1, C2, and C3 were close to the front cavity wall with vertical height H = 9.5, 31 and 42.5 mm, respectively. Points C12, C13, C14, and C15 were located close to the rear cavity wall at vertical height H = 42.5, 31, 19.5, and 10.5 mm, respectively. Points C4 to C11 were distributed uniformly from the front cavity wall to the rear cavity wall at vertical height H = 54.25 mm, in which C8 was located in the middle section of the impeller. The monitoring points in the diffuser (D1 – D11) are shown in Figures 4 (c) and (d). Points D1, D2, D3, and D4 were located along the flow direction in the outlet diffuser, whereas points D5, D6, and D7 were placed along the middle streamline of the corresponding flow channel in the return diffuser and intersected with a circle of radius R = 50, 40, and 25 mm, respectively. Points D8 and D9 were located on the blade pressure and suction sides of the return diffuser with

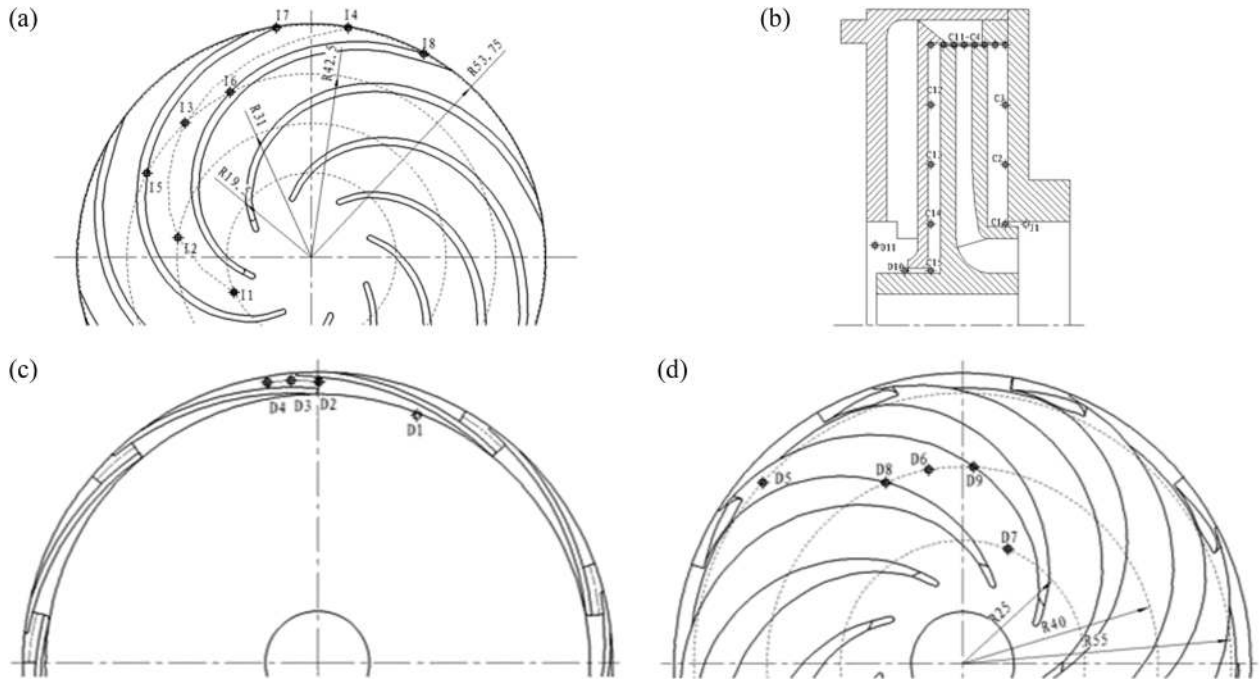

FIG. 4. Monitored points: (a) in the impeller; (b) in the pump cavity; (c) in the outlet diffuser; (d) in the return diffuser.

a circle radius R = 40 mm. Point J1 was located at the inlet of the front ring and corresponded to point C1, while D10 was located at the outlet of the rear ring and corresponded to point C15. Point D11 was located at the outlet of the return diffuser. Finally, the monitored points in the impeller were attached to the rotating coordinate system of the impeller and synchronously rotated with the impeller; in other words, they were stationary relative to the impeller.

III. PRESSURE DISTRIBUTION

Time- and frequency-domain analyses are generally used in processing the pressure fluctuation data. To remove the effect of the static pressure, the pressure fluctuation coefficient C_p was selected for the time- and frequency-domain analyses, which is defined as follows:

$$C_p = \frac{p - \overline{p}}{\frac{1}{2}\rho u_2^2} \tag{1}$$

Moreover, the standard deviation of pressure fluctuation, C_{RMS}, which is defined as follows, is used to represent the pressure fluctuating magnitude:

$$C_{RMS} = \frac{\sqrt{\frac{(p_1 - \overline{p})^2 + (p_2 - \overline{p})^2 + \cdots + (p_X - \overline{p})^2}{X}}}{\frac{1}{2}\rho u_2^2} \tag{2}$$

where p is the instantaneous point static pressure, Pa; $\overline{p}$ is the average point static pressure over one revolution period of the impeller, Pa; u_2 is the circumferential velocity at the outlet of the impeller, m/s; X is the number of time steps within one revolution of the impeller; and ρ is the density of the fluid, kg/m^3.

A. Pressure distribution at the impeller

The time history of the pressure fluctuation coefficient C_p at each monitored point (I1–I8) in the first- and second-stage impellers under the design flow condition is shown in Figure 5. The abscissa is the number of time steps (1 time step represents the time that the impeller rotates by 1°). The distribution of C_p at each monitored point shows nine similar waveforms during one revolution of the impeller. The time-domain distribution of C_p in the first-stage impeller is similar to that in the second-stage impeller. However, the absolute pressure inside the second-stage impeller is much higher than that in the first-stage impeller. Thus, no positive correlation exists between the amplitude of the pressure fluctuation coefficient and the absolute pressure value. As shown in Figures 5(a) and 5(b), the amplitude of C_p gradually increases from the impeller inlet to the outlet (I1–I4). Within the impeller, the pressure fluctuation coefficient shows an asymmetrical distribution about C_p=0: the positive C_p has a greater amplitude but a narrower distribution range than the negative C_p. Moreover, the distribution of C_p gradually becomes symmetrical near the impeller outlet. As shown in Figures 5(c) and 5(d), the amplitude of C_p gradually increases from the blade suction side to the blade pressure side at the same radius inside the impeller mainly because the wrap angle of the impeller blade is too large. The distance between the monitored point I5 (which is close to the blade pressure side) and the impeller outlet is considerably shortened. As shown in Figures 5(e) and 5(f), the amplitude of the positive C_p at I4 is noticeably smaller than that at I7 or I8, and the distribution of C_p in the middle of the impeller outlet depicts a good symmetry. Thus, the pressure fluctuation coefficient inside the impeller is significantly smaller than that at the impeller outlet. Inside the impeller the time step at which the peak or valley occurs is relatively stable, but at the impeller outlet it changes along the circumferential direction. Thus, the pressure fluctuation source of the fluid in the impeller arises from downstream of the impeller. The number of similar waveforms within one revolution of the impeller is equal to the number of outlet diffuser blades. Hence, the pressure fluctuation source of the fluid in the impeller must have arisen from the inlet edge of the outlet diffuser blade. The inside edge of each outlet diffuser blade represents a fluctuation source that interferes with the fluid inside the impeller.

The frequency-domain distribution of C_p at each monitored point from I1 to I8 in the first- and second-stage impellers under the design flow condition is shown in Figure 6. MP denotes the monitored points, and NF is a multiple of the rotating frequency of the impeller, that is, f_n = 2800/60 = 46.67 Hz. As shown in Figures 6(a) and 6(b), the frequency-domain pattern of C_p in the first-stage impeller is very similar to that in the second-stage impeller. However, there are some low frequency spikes in the second-stage impeller. The main frequency of C_p in the impeller is $9f_n$, which is also the blade frequency of the diffuser. Moreover, the amplitude of C_p is relatively large when the frequency is a multiple of $9f_n$. In general, the amplitude of C_p increases constantly from the impeller inlet to the impeller outlet. At a given position, the amplitude of C_p decreases to 0 as the frequency increases. One may observe from Figures 6(c) and 6(d) that the main frequency amplitude of C_p increases gradually from the blade suction side to the blade pressure side. Thus, the trend of the main frequency amplitude in the impeller is similar to that of the pressure fluctuation coefficient. As shown in Figures 6(e) and 6(f), the main frequency amplitudes of C_p at I4 and I7 are distinctly smaller than that at I8 at the same radius of the impeller outlet. Thus, the main frequency of C_p at each monitored point in the impeller is $9f_n$, and the frequency-domain distributions of C_p in the first- and second-stage impellers are essentially the same. The main frequency amplitude of C_p continues to increase from the impeller inlet to the impeller outlet. Thus, the pressure fluctuation of the fluid at the impeller arises from the inlet edge of the outlet diffuser blade.

The standard deviation of the pressure fluctuation coefficient C_{RMS} at each monitored point in the first-stage and second-stage impellers under different flow conditions is displayed in Figure 7. The distributions of C_{RMS} at the two impellers are nearly identical mainly because the two impellers have the same internal pressure gradient despite that the absolute pressure at the second-stage impeller is much higher. The value of C_{RMS} continues to increase from the impeller inlet to the impeller outlet. It also gradually increases from the blade suction side to the blade pressure side at the middle of the impeller. The increase of the flow rate leads to the continuous decrease of C_{RMS} within the impeller, particularly over the small flow rate range $Q/Q_{des} < 1.5$. The reason for this result is that the increase in the flow rate causes the overall pressure and pressure gradient inside the impeller to decrease together, thereby leading to the decrease of pressure fluctuation intensity at any point in the impeller. However, when Q/Q_{des} is large, the pressure fluctuation intensity increases sharply due to the excessive internal loss

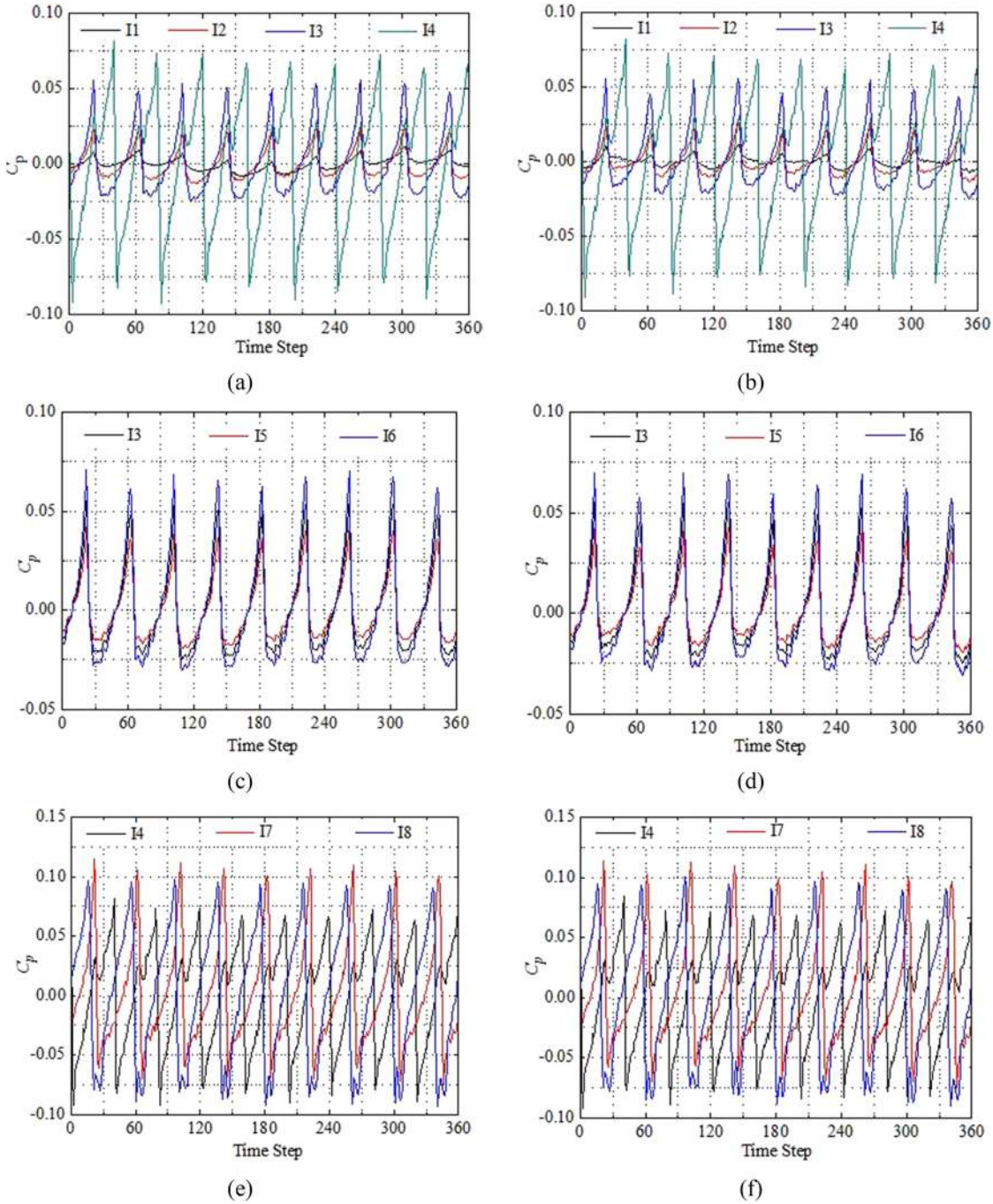

FIG. 5. Time-domain distribution of pressure fluctuation coefficient at each monitored point under design rated flow condition: (a), (c), (e) in the first-stage impeller; (b), (d), (f) in the second-stage impeller.

of the impeller pressure. Hence, the decrease rate in the impeller pressure under large flow condition is substantially reduced.

As shown in Figures 5–7, the pressure fluctuation of the fluid in the impeller arises from the inlet side of the outlet diffuser. Over one revolution of the impeller, any position in the impeller will pass by the nine blades of the outlet diffuser. Thus, the main frequency of the pressure fluctuation coefficient at any point in the impeller is $9f_n$. On the one hand, the larger the distance between the position in

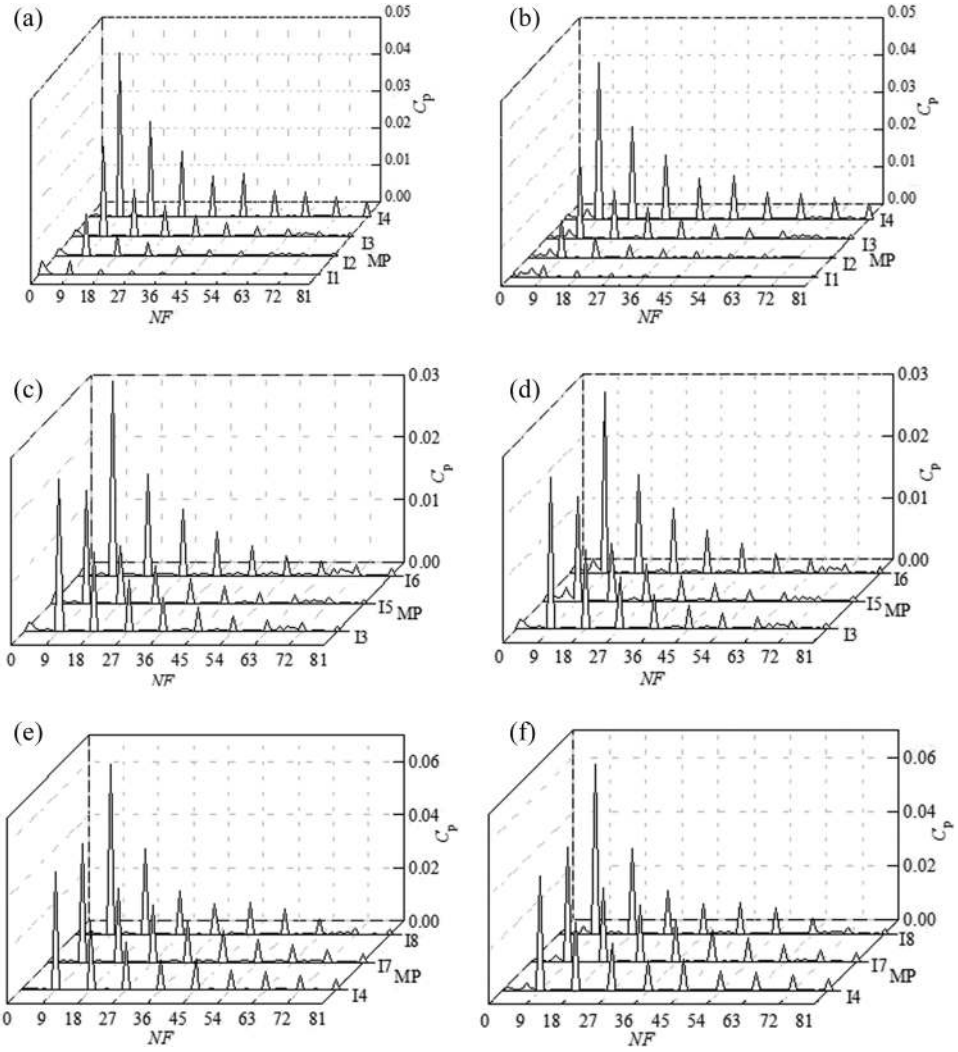

FIG. 6. Frequency-domain distribution of pressure fluctuation coefficient at each monitored point under the design flow condition: (a), (c), (e) in the first-stage impeller; (b), (d), (f) in the second-stage impeller.

the impeller and the inlet side of the outlet diffuser, the smaller the pressure fluctuation intensity at that point. At the position closest to the impeller inlet, the pressure fluctuation intensity is the minimum, and the main frequency of the pressure fluctuation coefficient is also the smallest. Thus, the fluid at the impeller inlet is the least affected by the inlet side of the outlet diffuser vane. On the other hand, the pressure fluctuation intensity at any point in the impeller is positively correlated with the pressure gradient but not with the

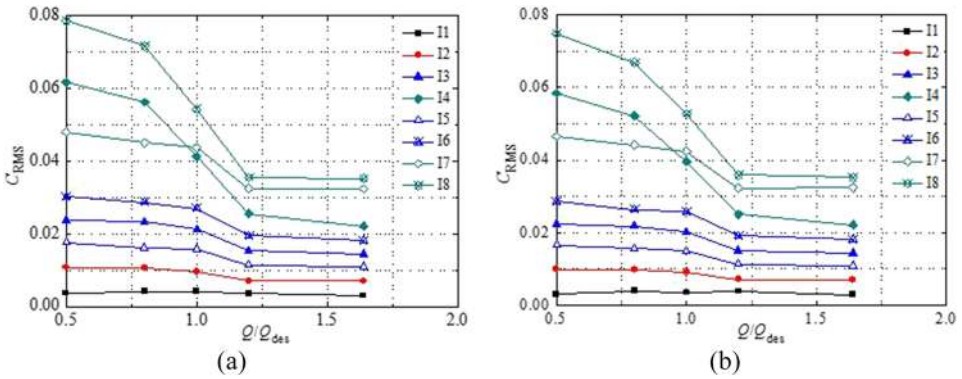

FIG. 7. Variation of standard deviation of pressure fluctuation coefficient with flow rate at each monitored point: (a) in the first-stage impeller; (b) in the second-stage impeller.

absolute pressure. The finding that the pressure fluctuation intensity does not simply increase with the number of pump stages is of great significance for studying the pressure fluctuation mechanism of a multistage centrifugal pump.

B. Pressure fluctuation analysis in the diffuser

The time-domain distribution of C_p at each monitored point in the first- and second-stage diffusers under the design flow condition is shown in Figure 8. The distribution of C_p at each monitored point exhibits eight similar waveforms over a full revolution of the impeller. The distribution of C_p in the first-stage diffuser is similar to that in the second-stage diffuser. As shown in Figures 8(a) and 8(b), the amplitude of C_p is much larger at D1 (which is not in the flow channel) than those at D2, D3, and D4 (which are in the flow channel). The value of C_p at each monitoring point toward the inside of the flow channel presents a symmetrical distribution. Almost similar time step positions exist, where the amplitude of C_p at each monitored point appears. The peak amplitude of C_p gradually decreases from the outlet diffuser inlet to the outlet. The amplitude decrease is rather small mainly because of the small radial size of the outlet diffuser. As shown in Figures 8(c) and 8(d), the amplitude of C_p also decreases gradually from the return diffuser inlet to the outlet, and the decrease rate reduces continuously. As shown in Figures 8(e) and 8(f), the amplitude of C_p gradually decreases from the blade suction side (D8) to the blade pressure side (D9) at the same radius in the middle of the diffuser. Thus, the pressure fluctuation coefficient in the diffuser is significantly lower than that in the impeller. The amplitude of the pressure fluctuation coefficient gradually decreases from the outward diffuser inlet to the return diffuser outlet. Throughout the whole diffuser, the time step location at the C_p peak and nadir inside the impeller is relatively stable. Thus, the pressure fluctuation source of the fluid in the diffuser arises from the upstream of the outlet diffuser. The number of waveforms during one revolution of the impeller is similar to the number of

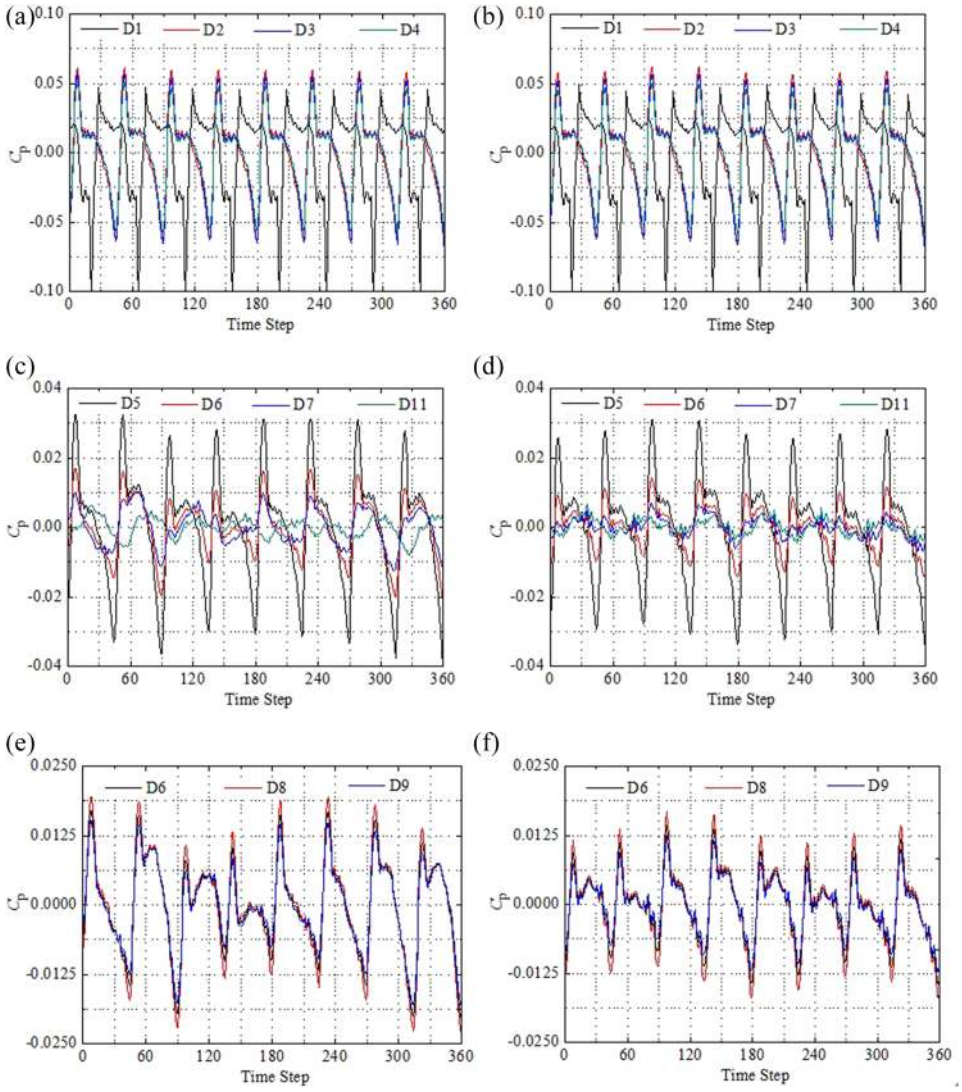

FIG. 8. Time-domain distribution of pressure fluctuation coefficient at each monitored point at the design flow condition: (a), (c), (e) in the first-stage diffuser; (b), (d), (f) in the second-stage diffuser.

impeller blades. Hence, the pressure fluctuation source of the fluid in the diffuser must have arisen from the outlet side of the impeller blade. In other words, the outlet side of each impeller blade is the pressure fluctuation source that interferes with the fluid inside the diffuser.

The frequency-domain distribution of C_p at each monitored point in the first- and second-stage diffusers at the design flow condition is presented in Figure 9. As shown in Figures 9(a) and 9(b), the frequency-domain distribution of C_p in the first-stage diffuser is nearly similar to that in the second-stage diffuser. The main frequency of C_p in the outlet diffuser is $8f_n$, which is also the impeller blade frequency. The amplitude of C_p is relatively large when the frequency is a multiple of $8f_n$. Moreover, the amplitude of C_p decreases to 0 alongside the increase in frequency, and it increases continuously from the outlet diffuser inlet (D1) to the outlet diffuser outlet (D4). As shown in Figures 9(c) and 9(d), the main frequency of C_p in the return diffuser is also $8f_n$, but the amplitude of the main frequency spike is considerably lower than that at the outward diffuser. The amplitude of the main frequency spike decreases continuously from the return diffuser inlet (D5) to the outlet (D7). At the diffuser outlet (D11), one may observe many low-frequency spikes (whose amplitudes exceed that of the impeller blade frequency) become the main frequency. As compared to the first-stage return diffuser, the main frequency amplitude of C_p in the second-stage diffuser is smaller and has more complex low-frequency spikes. According to Figures 9(e) and 9(f), the main frequency spike of C_p at D8 near the suction side of the return diffuser blade is the largest at the same radius of the return diffuser vane. By contrast, the main frequency amplitude of C_p at D9 on the pressure side is the smallest. In summary, the main frequency of the pressure fluctuation at each monitored point in the diffuser is the impeller blade frequency ($8f_n$). While the main frequency spike reduces continuously, the high-frequency spikes decrease constantly from the outlet diffuser inlet to the return diffuser outlet, and low-frequency spikes appear continuously. The main frequency of the pressure fluctuation at the monitoring point ceases to be $8f_n$ toward the outside of the return

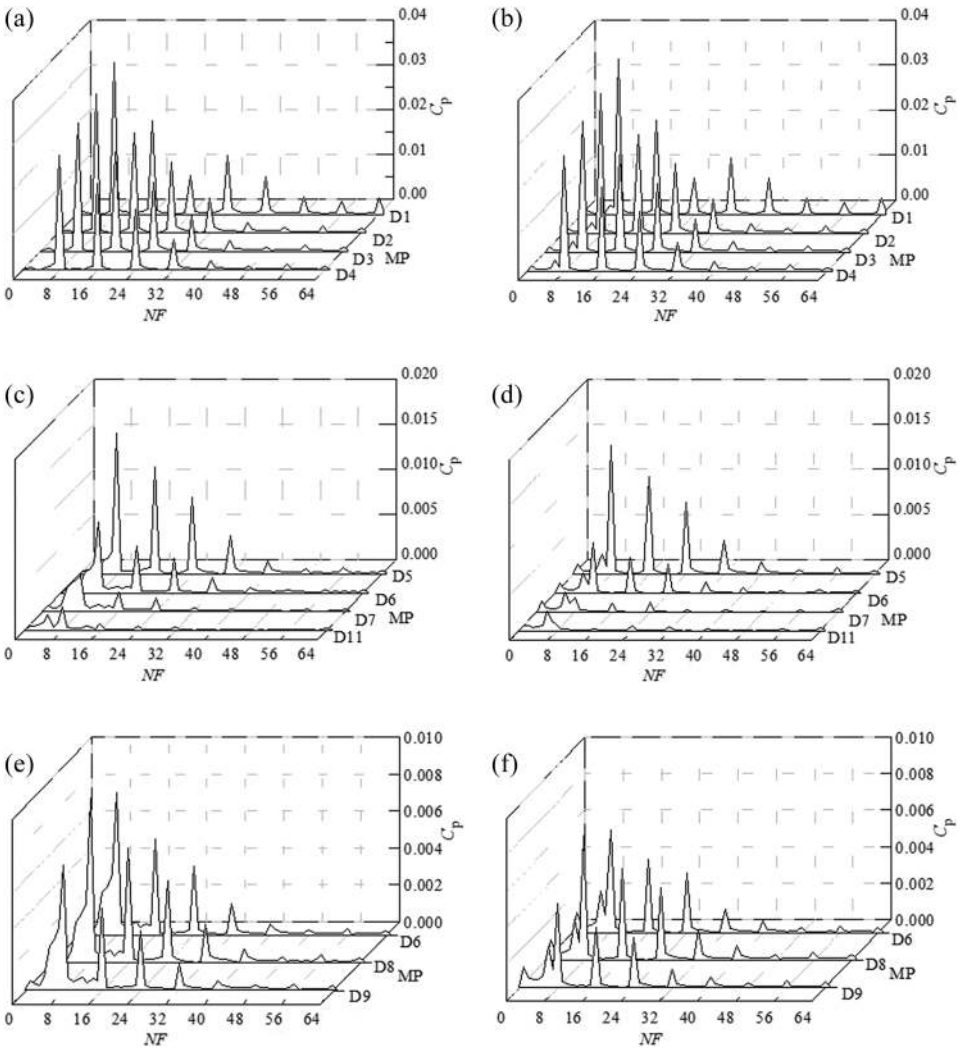

FIG. 9. Frequency-domain distribution of pressure fluctuation coefficient at each monitored point under rated flow condition: (a), (c), (e) in the first-stage diffuser; (b), (d), (f) in the second-stage diffuser.

diffuser. Thus, the pressure fluctuation in the diffuser arises from the outlet edge of the impeller blade. The effects of this disturbance become minimal toward the return diffuser outlet.

The variation of C_{RMS} with flow rate in the first- and second-stage diffusers is shown in Figure 10. Similar to the distribution of C_p, C_{RMS} in the first-stage diffuser is nearly similar to that in the second-stage diffuser. The value of C_{RMS} decreases continuously by approximately 20% from the outward diffuser inlet (D1) to the outlet (D4). By contrast, the value of C_{RMS} decreases rapidly by 30% from the outward diffuser outlet (D4) to the return diffuser inlet (D5). Thus, the intensity of pressure fluctuation is substantially reduced at the transition region between the outward diffuser and the return diffuser. Meanwhile, C_{RMS} decreases by approximately 40% from the return diffuser inlet (D5) to the outlet (D11). Therefore, the value of C_{RMS} at the return diffuser outlet is less than 10% of that at the outward diffuser inlet. The value of C_{RMS} in the diffuser increases with flow rate, and especially in the outward diffuser. The reason is that the pressure fluctuation intensity in the flow field is related not only to the pressure gradient of the position itself and the distance from the fluctuation source, but also to the instability of flow field. The more unstable the flow, the greater the turbulence kinetic energy and the pressure fluctuation intensity (and hence the standard deviation). The radial size of the outlet diffuser is too small, and its capacity is very small. Hence, the head loss at the diffuser increases sharply with flow rate, resulting in increased turbulence kinetic energy and pressure fluctuation in the diffuser. The pressure gradient in the diffuser decreases with flow rate, thereby weakening the pressure fluctuation intensity to a certain extent. However, the increased pressure fluctuation intensity because the flow instability is significant. Ultimately, the standard deviations of pressure fluctuation in the diffuser increase with flow rate, especially under large flow conditions.

As shown in Figures 8–10, the pressure fluctuation of the fluid in the diffuser arises from the outlet side of the impeller blade. During a full revolution of the impeller, any point in the diffuser passes by eight impeller blades. Hence, the main frequency of the pressure fluctuation coefficient in the diffuser is $8f_n$. On the one hand, the further from the outlet of the impeller blade, the smaller the pressure fluctuation intensity. The pressure fluctuation intensity at the return diffuser outlet reaches the minimum, and the main frequency of the pressure fluctuation coefficient also becomes small. Thus, the fluid at the return diffuser outlet is less affected by the impeller blade outlet. On the other hand, the pressure fluctuation intensity at any position in the diffuser is positively correlated with the pressure gradient and flow instability.

C. Pressure distribution in the pump volute

The time-domain distribution of C_p at each monitored point in the first- and second-stage pump cavities under the design flow condition is shown in Figure 11. Each profile displays as eight similar waveforms over a full revolution of the impeller, and the periodicity of C_p in the first-stage pump volute is more significant than that in the second-stage pump volute. According to Figures 11(a) and 11(b), the amplitude of C_p at each monitored point in the front pump volute is significantly smaller than that in the impeller or diffuser. As the diameter of the pump volute increases, the amplitude of C_p in the front pump volute gradually increases and reaches the maximum at C4, which is near the impeller outlet. As shown in Figures 11(c) and 11(d), the amplitude of C_p at C11 near the impeller outlet is much larger than that at the other monitored points in the rear pump volute. The reason for this result is that the fluid leaving the impeller outlet does not directly flow into the rear pump volute, thereby causing the pressure fluctuation intensity to decay rapidly. As shown in Figures 11(e) and 11(f), the amplitude of C_p at C8 (at the cross section of the impeller) reaches the maximum in the upper pump volute between the impeller and the diffuser. Given that the monitored point is far from the cross section, the amplitude of C_p gradually decreases and reaches the minimum near the front and rear pump walls. However, the pressure fluctuation coefficient at the monitored point in the pump volute retains a certain periodicity. The pressure pulsation of the fluid in the front pump volute and the upper pump volute arises from the outlet side of the impeller blade. Meanwhile, the pressure pulsation source of the fluid in the rear pump volute is due to the interstage leakage fluid from the return diffuser outlet to the rear pump volute.

The frequency-domain distribution of C_p at each monitored point in the first- and second-stage pump cavities under the design flow condition is shown in Figure 12. According to Figures 9(a) and 9(b), the main frequency of C_p in the front pump volute is $8f_n$, which is also the impeller blade frequency. The amplitude of C_p is quite significant when the frequency is a multiple of $8f_n$. The frequency-domain distribution of C_p in the first-stage pump volute is nearly similar to that in the second-stage pump volute, except that many low-frequency spikes appeared in the second-stage pump volute. As shown in Figures 12(c) and 12(d), the main frequency of C_p in the rear pump volute (except at C11 which is closest to the impeller

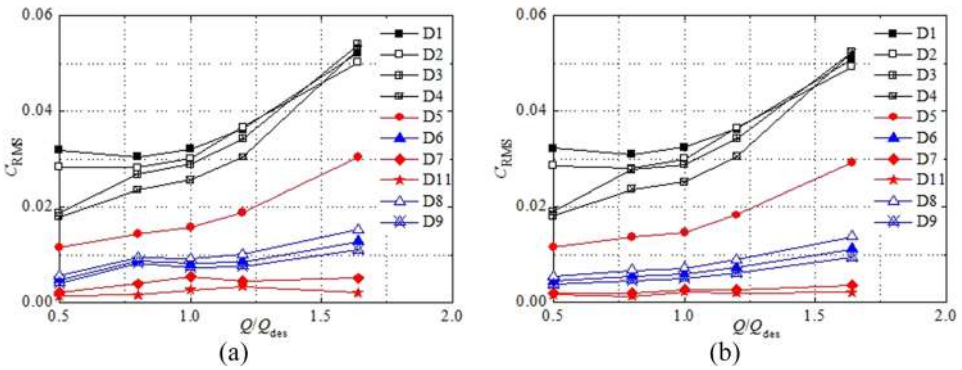

FIG. 10. Variation of standard deviation of pressure fluctuation coefficient with flow rate at each monitored point: (a) in the first-stage diffuser; (b) in the second-stage diffuser.

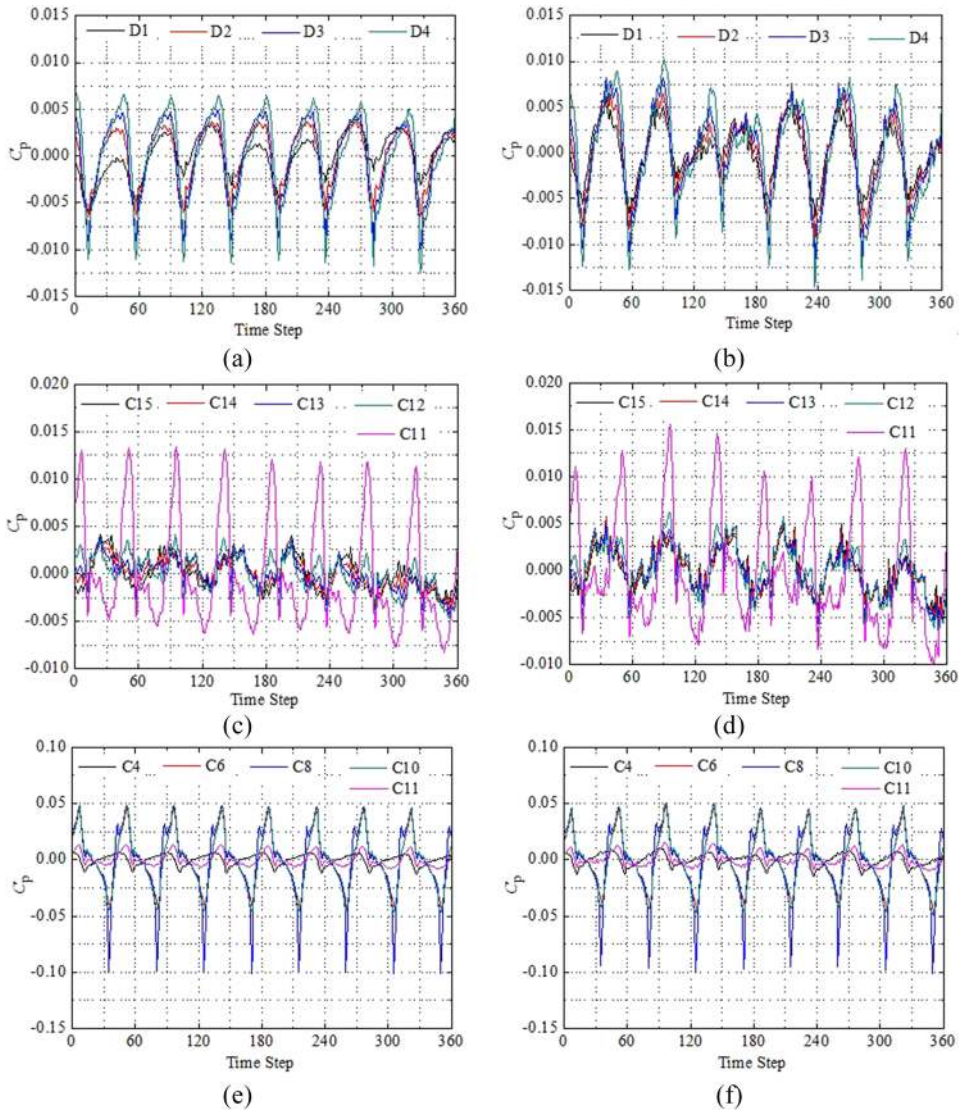

FIG. 11. Time-domain distribution of pressure fluctuation coefficient at each monitored point at the design condition: (a), (c), (e) in the first-stage pump volute; (b), (d), (f) in the second-stage pump volute.

outlet) is $8f_n$ (low frequency). In addition, the amplitude of C_p at C11 is much larger than that at the other monitored points; this condition largely differs from the general trend in the front pump volute. In Figures 12(e) and 12(f), the main frequency of C_p is $8f_n$ in the upper pump volute between the impeller and the diffuser. In summary, the main frequency of the pressure fluctuation coefficient is $8f_n$ as the fluid leaves the impeller. The main frequency amplitude decreases rapidly when the fluid flows to the pump volute. The main frequency of the pressure fluctuation coefficient in the front pump volute is also $8f_n$ because the fluid in the front pump cavity originates from the impeller outlet and flows into the impeller inlet through the front ring. Moreover, the main frequency of the pressure fluctuation coefficient at C15, which is near the interstage ring, becomes $8f_n$ as the fluid at the return diffuser outlet returns to the rear pump volute through the interstage ring; this activity is consistent with that at D11 (near the return diffuser outlet).

The standard deviation of the pressure fluctuation coefficient C_{RMS} in the first- and second-stage pump cavities under different flow conditions is shown in Figure 13. The distribution of C_{RMS} in the first-stage pump volute is nearly similar to that in the second-stage pump volute, and C_{RMS} continuously increases with flow rate. The value of C_{RMS} at C8, which located at the cross section of the impeller, is the largest in the upper pump volute. Given that the monitored point is far from the cross section, the value of C_{RMS} gradually decreases and reaches the minimum when it is near the front and rear pump walls. The values of C_{RMS} at C4 and C11 are only 1/5 of that at C8. Thus, the pressure fluctuation intensity in the upper pump volute decays remarkably rapidly along the axial direction. In the front pump volute, C_{RMS} decreases gradually and reaches the minimum at C1 near the front ring as the diameter of the pump volute decreases. With increasing flow rate, the fluid through the front pump volute and the front ring decreases instead

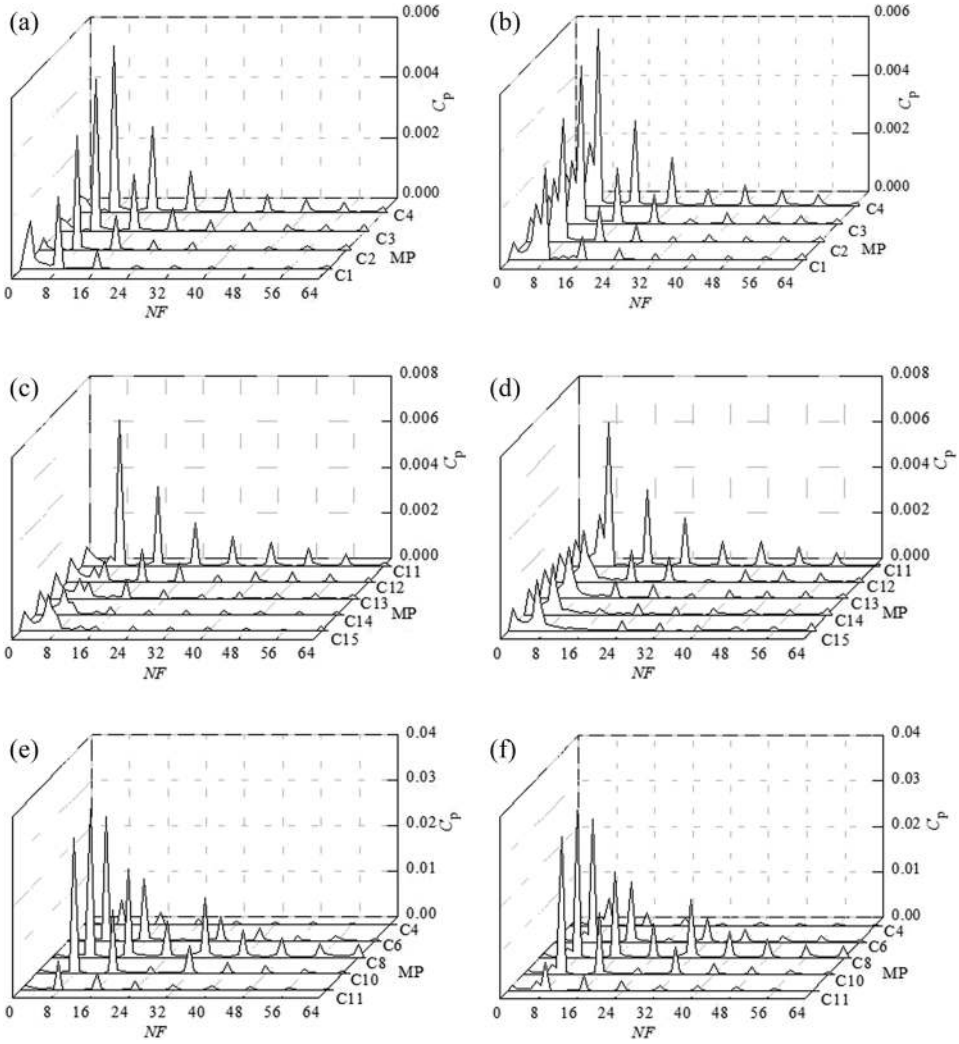

FIG. 12. Frequency-domain distribution of pressure fluctuation coefficient at each monitored point under rated flow condition: (a), (c), (e) in the first-stage pump volute; (b), (d), (f) in the second-stage pump volute.

due to the decrease in the pressure difference. Moreover, C_{RMS} in the front pump volute decreases quickly. In the rear pump volute, C_{RMS} decreases rapidly and then remains constant as the diameter of the pump volute decreases. The trends of C_{RMS} in the front and rear pump volutes are affected by the fluid passing through relevant flow regions.

According to Figures 11–13, two pressure fluctuation sources affect the fluid in the pump volute, namely, the outlet of the impeller

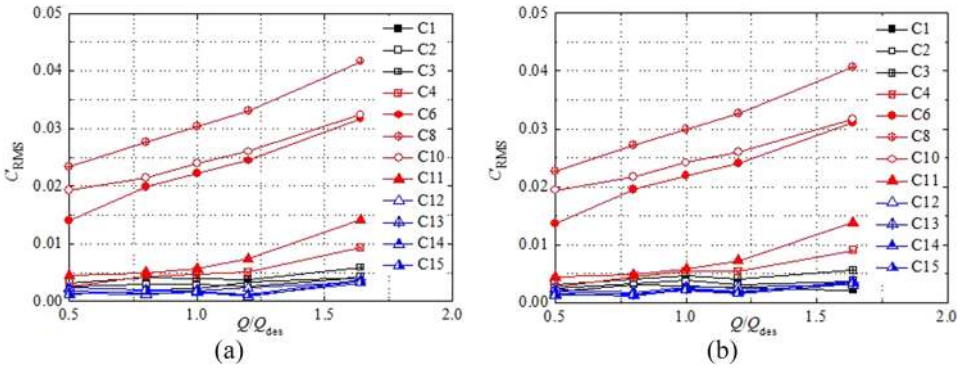

FIG. 13. Variation of standard deviation of pressure fluctuation coefficient with flow rate at each monitored point: (a) in the first-stage pump volute; (b) in the second-stage pump volute.

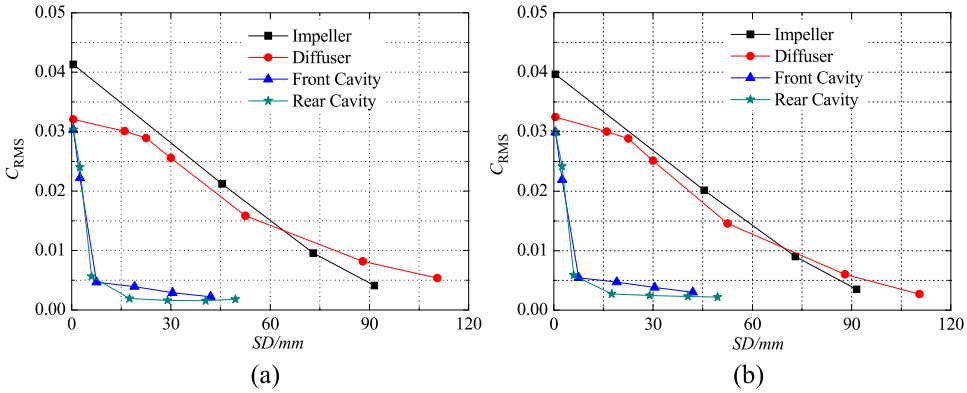

FIG. 14. Variation of standard deviation of pressure fluctuation coefficient with streamline distance (SD) at each monitored point under the design flow condition: (a) in the first-stage pump; (b) in the second-stage pump.

blade and the interstage leakage fluid from the return diffuser outlet to the rear pump volute. The fluid in the front and the upper pump volutes is affected by the outlet side of the impeller blade, and the main frequency is $8f_n$. The fluid in the rear pump volute is affected by the outlet side of the impeller blade and the interstage leakage. Moreover, the interstage leakage plays a major role in the rear pump volute, and the main frequency is $8f_n$, which is similar to that of the fluid in the return diffuser outlet.

D. Pressure distribution in the pump

The standard deviation of the pressure fluctuation coefficient C_{RMS} in the first- and second-stage pumps under the design flow condition is shown in Figure 14. The abscissa is the streamline distance (SD) between the monitored point and the fluctuation source in the pump. The monitored points in the impeller are successively I4, I3, I2, and I1; the monitored points in the diffuser are D1, D2, D3, D4, D5, D6, and D7; the monitored points in the front pump volute are C8, C6, C4, C3, C2, and C1; and the monitored points in the rear pump volute are C8, C10, C11, C12, C13, C14, and C15. The distributions of C_{RMS} in the two stages are basically the same. The value of C_{RMS} decreases continuously with the increase in SD. The decrease rate in the diffuser is the smallest, whereas that in the pump volute is the largest. The decrease rate of C_{RMS} in the impeller is almost linear. The decrease rate of C_{RMS} in the diffuser is varied because the shape of the transition region between the outward diffuser and the return diffuser is rather complex: it is small in the outward diffuser, then becomes larger in the transition region, and becomes smaller in the return diffuser. Given the inverted "L" shape of the front pump volute, the decrease rate of C_{RMS} in the front pump volute decreased rapidly and then decreases gradually radially. The decrease rate of C_{RMS} in the front pump volute is rapidly reduced axially and then remains stable radially because of the interstage leakage in the rear pump volute. Therefore, the pressure fluctuation is mainly transmitted through the fluid. The decay rate of C_{RMS} would be excessively small if the flow between any position and the fluctuation source is large (main stream) and the position is downstream of the fluctuation source. If the flow between the position and the fluctuation source is large (main stream) and the position is upstream of the fluctuation source, then the decay rate of C_{RMS} would be moderate. Finally, C_{RMS} would decay rapidly if the flow between the position and the fluctuation source is remarkably small or the connection between the position and the fluctuation source is not aligned or coincident with the plane movement of the fluctuation source.

The mathematical expression of the pressure fluctuation coefficient is essentially a wave, which is determined by three important factors including the amplitude (intensity), frequency, and phase. In the literature on pressure fluctuation, the amplitude and frequency have been reported and analyzed while the phase was ignored. The phase distribution of pressure fluctuation coefficient wave is comprehensively studied in this paper. The large cycle has a total of 360 time steps during one impeller revolution because the one-degree impeller rotation is set as one time step. Moreover, the small cycle has 45 time steps because the number of the impeller blade is 8.

Figure 15 shows the phase distribution of C_p at the monitored points in the first-stage impeller and diffuser during two small cycles

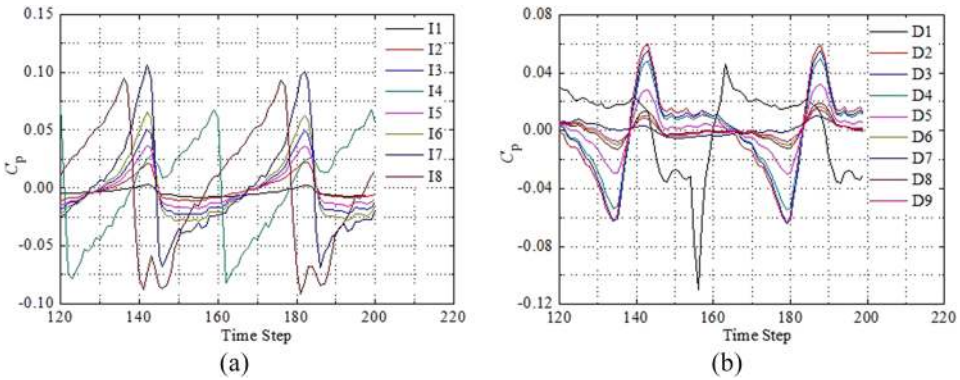

FIG. 15. Phase distribution of pressure fluctuation coefficient at each monitored point under rated flow condition: (a) in the first-stage impeller; (b) in the first-stage diffuser.

under the design flow condition. In Figure 16, the static pressure distribution in the mid-section is superimposed to illustrate the phase change of C_p more clearly. Figure 15(a) shows that in the entire impeller, except for I4, I7, and I8 at the impeller outlet, the phases of C_p at the five other monitored points are exactly the same, and with the peak and trough occurred at time steps of 142 and 153, respectively. In addition, the time step for I7 to attain the peak is 142, whereas those for I4 and I8 have lagged to 159 and 176, respectively. As in Figures 16(d) and 16(f), at time step 142 when I7 is close to the inlet side of the outlet diffuser vane, the impeller flow channel is fully docked with the outlet diffuser flow channel. Hence, the flow resistance in the impeller reaches the minimum, and the static pressure at all the monitored points in the impeller (excluding I4 and I8) simultaneously reaches the maximum. Moreover, due to the large wrap angle of impeller blade, the outlet angle (19°) of the suction side of the impeller blade is larger than that (15°) at the pressure side. As a

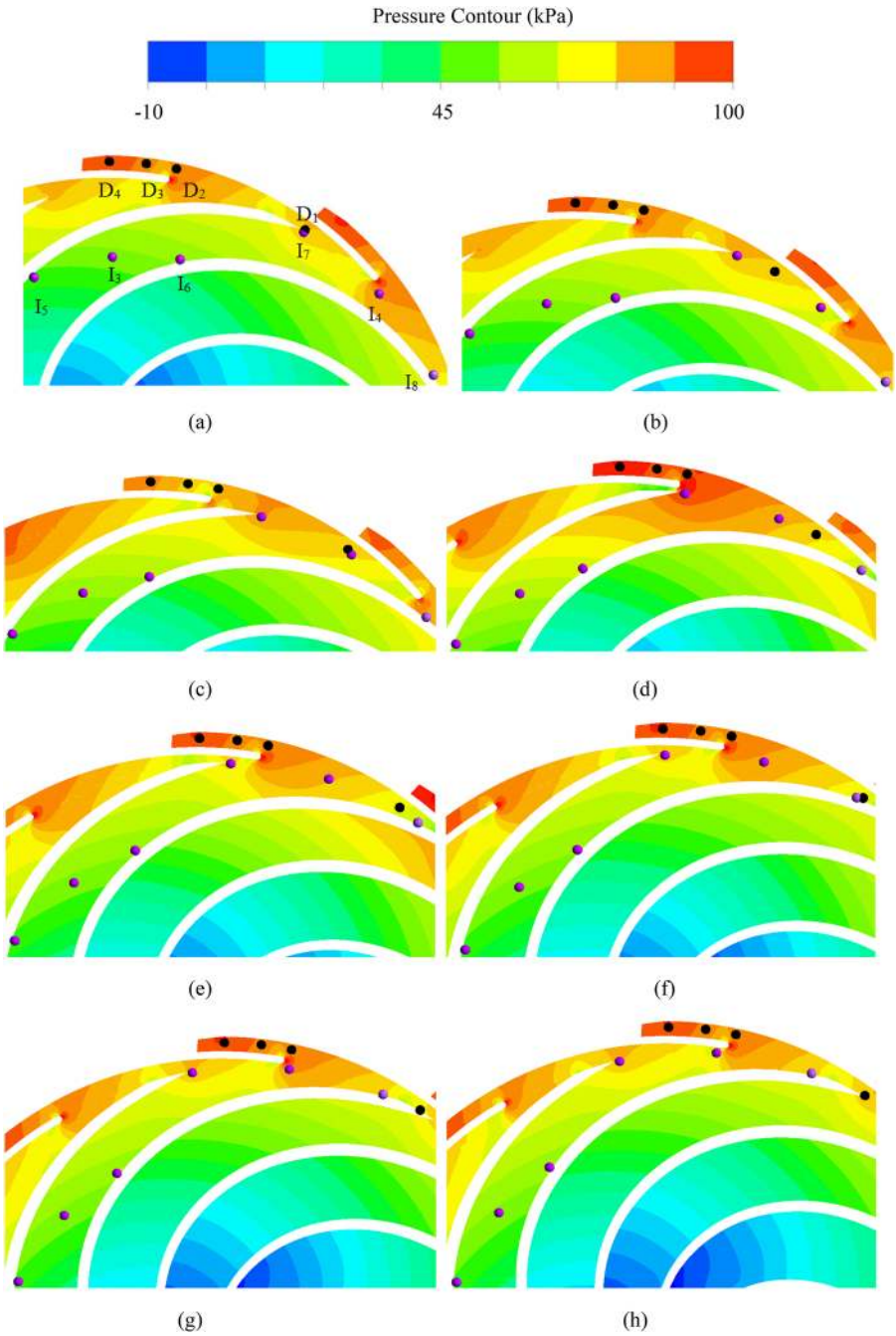

FIG. 16. Pressure distribution in the first-stage impeller and diffuser under rated flow condition when time step equals to: (a) 118; (b) 125; (c) 134; (d) 142; (e) 148; (f) 153; (g) 159; (h) 161.

result, the flow capacity near the suction side of the impeller blade is stronger than that near the pressure side. Therefore, at time step 153, the inlet side of the outward diffuser is not at the geometric center of the impeller flow channel, but at the exact center of liquid flow passing through the impeller flow channel. At this time step, the internal flow resistance in the impeller is at its maximum, and the static pressure of C_p at all the monitored points in the impeller (excluding I4, I7, and I8) correspondingly reaches the minimum. As I4 and I8 are respectively close to the inlet side of the positive diffuser at the time steps of 159 and 176, the static pressure reaches the maximum.

As shown in Figure 15(b), except for point D1 that is not located in the flow channel of the outlet diffuser, the phases for the other eight monitored points (D2 to D9) in the diffuser are completely the same, and the time steps attaining the peak and trough are 142 and 134, respectively. Figures 16(c) and 16(d) show that, due to larger outlet angle of the suction side of the impeller blade than that at the pressure side, the high-pressure region is near the suction side of the impeller blade outlet, while the low-pressure region appears near the pressure side. When the time step is 134, the low-pressure region sweeps through the monitored points in the flow channel of the outward diffuser vane. As a result, the static pressure at each monitored point in the outward diffuser (excluding D1) reaches the minimum, corresponding to the trough in the pressure coefficient distribution. By contrast, at time step 142, the high-pressure region sweeps through the monitored points in the outward diffuser (excluding D1), causing the pressure to peak.

As shown in Figure 17, the phase distribution of pressure fluctuation coefficient in the impeller and diffuser can be divided into four regions: the impeller flow channel region (I), the impeller transition region (II), the diffuser transition region (III), and the diffuser flow channel region (IV). The pressure fluctuation sources of the liquid in regions I and II are located at both the inlet side of the outward diffuser, whereas those in regions III and IV originate from both the outlet side of the impeller blade. Meanwhile, the phases of pressure fluctuation coefficient in region I or IV are nearly the same. When the inlet side of the outlet diffuser blocks the impeller flow channel, the amplitude of pressure fluctuation coefficient in region I is relatively small. When the suction side of the impeller blade outlet (high-pressure region) sweeps through the outward diffuser flow channel, the amplitude of pressure fluctuation coefficient in region IV reaches the maximum, and the trend is transmitted to the return diffuser flow channel. Moreover, the phases of pressure fluctuation coefficient in regions II and III differ from each other; a phase close to the inlet side of the outlet diffuser or the suction side of the impeller blade outlet leads to small time step number for the pressure fluctuation coefficient to reach the peak.

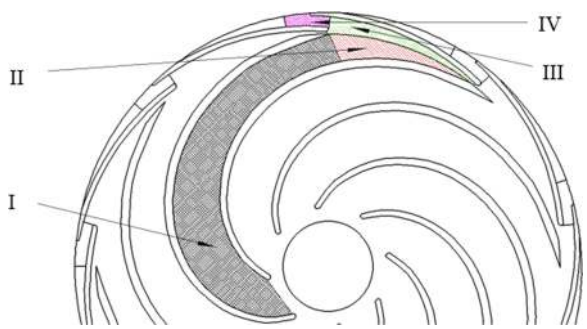

FIG. 17. Phase region of pressure fluctuation in the first-stage impeller and diffuser under rated flow condition.

IV. CONCLUSIONS

(1) The pressure fluctuation of the fluid in the impeller comes from the inlet side of the outward diffuser, which corresponds to a fluctuation source that interferes with the fluid inside the impeller. Meanwhile, the pressure fluctuation of the fluid in the diffuser arises from the outlet of the impeller blade, which acts as a fluctuation source that interferes with the fluid inside the diffuser. Therefore, the outlet side of the impeller blade and the interstage leakage fluid are the sources of pressure fluctuation in the pump volute.

(2) Pressure fluctuation is essentially a wave with distinct amplitude (intensity), frequency, and phase. Four main factors that influence the intensity of the pressure fluctuation at any position in the pump: the distance from the fluctuation source, the pressure gradient, the flow instability, and the relative orientation with respect to the fluctuation source. The pressure fluctuation intensity at any position is positively correlated with the pressure gradient and turbulence kinetic energy, and negatively correlated with the distance from the source of the fluctuation. The relative orientation with respect to the fluctuation source influences the strength of the negative correlation. That is, if the position is located in the downstream of the fluctuation source, then the fluctuation intensity will decay slowly with distance. Moreover, two main factors influence the pressure fluctuation frequency in the pump, i.e., the number of fluctuation sources and the rotational speed of the impeller. The main frequency of the pressure fluctuation in the impeller corresponds to the diffuser blade frequency, whereas that in the diffuser and the pump volute corresponds to the impeller blade frequency. Finally, two main factors affect the phase of pressure fluctuation in the pump, namely, the location and distance between from the fluctuation source. The phase distribution of the pressure fluctuation wave in the impeller and diffuser can be divided into four regions: the impeller flow channel, the impeller transition, the diffuser transition, and the diffuser flow channel regions. The pressure fluctuation phases in the impeller flow channel region or in the diffuser flow channel are nearly the same, whereas those in the impeller transition region or in the diffuser transition region differ.

ACKNOWLEDGMENTS

This work was supported by the funding for the National Natural Science Foundation of China (Grant No. 51609105), China Postdoctoral Science Foundation (Grant No. 2016M601738) and China Postdoctoral Science Foundation (Grant No. 2018T110458).

REFERENCES

[1] C. Wang, W. Shi, X. Wang *et al.*, "Optimal design of multistage centrifugal pump based on the combined energy loss model and computational fluid dynamics," Applied Energy **187**, 10–26 (2017).

[2] Z. Lu, Q. Liu, K. Wang *et al.*, "Worldwide technical analysis on multistage centrifugal pump based on patent map," Journal of Drainage and Irrigation Machinery Engineering **35**(3), 216–221 (2017).

[3] R. Xie, F. Tang, S. Li *et al.*, "Cross-section unbalanced force among impellers of five-stage centrifugal pump," Journal of Drainage and Irrigation Machinery Engineering **35**(10), 842–848 (2017).

[4] C. Wang, X. Chen, N. Qiu *et al.*, "Numerical and experimental study on the pressure fluctuation, vibration, and noise of multistage pump with radial diffuser," Journal of the Brazilian Society of Mechanical Sciences and Engineering **40**(10), 481 (2018).

[5] Z. Lu, C. Wang, N. Qiu *et al.*, "Experimental study on the unsteady performance of the multistage centrifugal pump," Journal of the Brazilian Society of Mechanical Sciences & Engineering **40**(5), 264 (2018).

[6] G. Lin, J. Yuan, Q. Si *et al.*, "Effect of impeller geometric parameters on characteristics of inlet recirculation in centrifugal pump," Journal of Drainage and Irrigation Machinery Engineering **35**(2), 106–112 (2017).

[7] Q. Li and M. Liu, "Flow characteristic of guide vane region in turbine braking operation of pump-turbine," Journal of Drainage and Irrigation Machinery Engineering **35**(6), 495–501 (2017).

[8] L. Tan, W. Shi, D. Zhang *et al.*, "Numerical and experimental investigations on the hydrodynamic radial force of single-channel pumps," Journal of Mechanical Science and Technology **32**(10), 4571–4581 (2018).

[9] X. Li, P. Gao, Z. Zhu *et al.*, "Effect of the blade loading distribution on hydrodynamic performance of a centrifugal pump with cylindrical blades," Journal of Mechanical Science and Technology **32**(3), 1161–1170 (2018).

[10] X. Li, Z. Jiang, Z. Zhu *et al.*, "Entropy generation analysis for the cavitating head-drop characteristic of a centrifugal pump," Proceedings of the Institution of Mechanical Engineers, Part C: Journal of Mechanical Engineering Science, 2018.

[11] R. P. Dring, H. D. Joslyn, L. W. Hardin *et al.*, "Turbine rotor-stator interaction," Journal of Engineering for Gas Turbines and Power **104**(4), 729–742 (1982).

[12] N. Arndt, A. J. Acosta, C. E. Brennen *et al.*, "Rotor-stator interaction in diffuser pump," ASME Journal of Turbomachinery **111**(3), 213–221 (1989).

[13] X. He, "The mechanism on forming of the pressure pulse in vane pump," Mechanical Science and Technology for Aerospace Engineering **25**(6), 38–42 (1996).

[14] N. Arndt, A. J. Acosta, C. E. Brennen *et al.*, "Experimental investigation of rotor-stator interaction in a centrifugal pump with several vaned diffusers," ASME Journal of Turbomachinery **112**, 98–108 (1990).

[15] N. He, M. Tan, H. Liu *et al.*, "Test and analysis on pressure pulsation and hydraulic performance of saddle zone in axial flow pump," Journal of Drainage and Irrigation Machinery Engineering **36**(2), 118–123 (2018).

[16] J. Feng, F. K. Benra, and H. J. Dohmen, "Unsteady flow investigation in rotor-stator interface of a radial diffuser pump," Forschung im Ingenieurwesen **74**(4), 233–242 (2010).

[17] G. Li and C. Lu, "Experiment on pressure fluctuation of kaplan turbine with low specific speed," Journal of Drainage and Irrigation Machinery Engineering **35**(10), 869–873 (2017).

[18] C. Wang, S. Wu, W. Shi *et al.*, "Numerical calculation and experimental research of pressure fluctuation in the pump under different operating conditions," Journal of Vibroengineering **15**(4), 2049–2056 (2013).

[19] M. Tan, Y. Lan, X. Wu *et al.*, "Unsteady dynamics in double channel pump," Journal of Drainage and Irrigation Machinery Engineering **35**(12), 1024–1029 (2017).

[20] Z. Liu, F. Kong, Y. Wang *et al.*, "Effect of unequal spacing blade distribution on pressure fluctuation of self-priming vortex pump," Journal of Drainage and Irrigation Machinery Engineering **35**(2), 113–118 (2017).

[21] F. Wang, L. Zhang, and Z. Zhang, "Analysis on pressure fluctuation of unsteady flow in axial-flow pumps," Journal of Hydraulic Engineering **38**(8), 1003–1009 (2007).

[22] D. Zhang, W. Shi, X. Guan *et al.*, "Investigations of unsteady flow field characters in axial flow pump based on numerical simulation," Proceedings of the ASME - JSME - KSME 2011 Joint Fluids Engineering Conference, Hamamatsu, Shizuoka, Japan.

[23] L. Ji, W. Li, W. Shi *et al.*, "Influence of different blade numbers on unsteady pressure pulsations of internal flow field in mixed-flow pump," Journal of Drainage and Irrigation Machinery Engineering **35**(8), 666–673 (2017).

[24] Y. Gu, S. Yuan, J. Pei *et al.*, "Effects of diffuser installation position on pressure fluctuation in the mixed flow pump," Journal of Drainage and Irrigation Machinery Engineering **35**(2), 93–99 (2017).

[25] D. Han, F. Yu, and S. Zhang, "Numerical simulation of unsteady three-dimensional flow in turbine mode of a pump-turbine," Journal of Drainage and Irrigation Machinery Engineering **35**(4), 325–332 (2017).

[26] G. Shi, X. Liu, W. Wei *et al.*, "Pressure pulsation characteristics in pump as hydraulic turbine with guide vanes," Journal of Drainage and Irrigation Machinery Engineering **35**(1), 6–12 (2017).

[27] F. Shi and H. Tsukamoto, "Numerical study of pressure fluctuations caused by impeller-diffuser interaction in a diffuser pump stage," ASME Journal of Fluids Engineering **123**(3), 466–474 (2001).

[28] H. Liu, X. Zhou, K. Wang *et al.*, "Analysis on pressure fluctuation of radial diffusers in a multistage centrifugal pump," Journal of Central South university (Science and Technology) **45**(9), 3295–3330 (2014).

[29] W. Shi, Y. Xu, Q. Zhang *et al.*, "Characteristics of pressure pulsation in multi-stage submersible pump," Journal of Drainage and Irrigation Machinery Engineering **32**(3), 196–201 (2014).